

RESEARCH

Open Access



# The effect of inhibiting molybdate used in anodizing-conversion treatment to improve corrosion protection of AA2030 aluminum alloy in different steps

Manel Benmohamed<sup>1\*</sup>, Abdelbaki Benmounah<sup>1</sup>, Ahmed Haddad<sup>2</sup> and Sarah Yahi<sup>3</sup>

\*Correspondence:  
m.benmohamed@univ-boumerdes.dz

<sup>1</sup> University M'hamed Bougara, Faculté des Sciences de l'Ingénieur (Campus ouest-Boumerdès) Cité Frantz, Fanon 35000 Boumerdès, Algeria  
Full list of author information is available at the end of the article

## Abstract

In this article, different treatment baths for corrosion protection of 2030 aluminum alloy in addition to replacing the hexavalent chromium due to the European recommendation were employed. This work is divided into three steps of treatment: first, anodization using molybdate inhibitor without and with phosphoric acid and, then, pre-oxidation with sodium hydroxide. In the last step, we studied the influence of conversion coating with the combination of sodium molybdate and fluoride on the anodic layer formed on aluminum alloy 2030. In order to characterize the formed layers, we use microstructural characterization (SEM, AFM, and nano-indentation), which allows highlighting the surface condition as well as the morphological distribution, and electrochemical techniques such as potentiodynamic polarization and electrochemical impedance spectroscopy which shows that the anodization treatment of the aluminum alloy with phosphoric acid and sodium molybdate offered better corrosion resistance. This resistance increased with the use of pre-oxidation and then reached a maximum value of 99.8% efficiency with the addition of the molybdate conversion coating which causes an increase in the double layer and gave an alternative possibility of chromium VI.

**Keywords:** Corrosion, Anodization, Sodium molybdate, Electrochemical impedance spectroscopy, Potentiodynamic polarization

## Introduction

Alumina is a spontaneously formed surface layer in the natural state, and upon exposure to the atmosphere, as soon as the environment becomes aggressive [1], the metal surface acquires an electrical potential that causes the migration of metal ions into the solution in the form of the cations, and this mechanism accounts for the corrosion of the metal in the electrolyte [2].

Corrosion is a natural phenomenon, but it represents a big problem in the transportation industry because it causes the erosion of metals [3]. Aluminum and its alloys are the metals most used in the aeronautical field [4]; they have low density, low electrical

conductivity, and good mechanical properties; and they offer great resistance to corrosion [5, 6]. Aluminum of the 2030 series (Al-Cu-Mg-Pb) is an anodic alloy which has a very negative redox potential which causes the formation of an inert protective layer [7]. In order to improve the strength of the aluminum alloy and increase the protection against pitting corrosion (localized corrosion), several mechanical, chemical, and electrochemical methods have been carried out [8–12]. Anodizing, coatings, and inhibitors are used to develop a passive, conductive, and protective artificial layer which improves the physical and chemical properties of aluminum in inorganic electrolytes [13].

The electrochemical anodization process is more used in the surface treatment industry, it causes the formation of a thin film of alumina and improves its adhesion to aluminum alloy [14], and its thickness and structure are controlled by different parameters (time, temperature, flow rate, and composition of the bath) [15]. This treatment is an electrochemical conversion process which forms relatively dense barrier/porous-type oxide layers with a decorative appearance and higher resistance to corrosion and scratches [16–18], thus providing better adhesion of the alumina formed from the base material [8]. According to Yen et al., the surface structure of micro/nano-complex aluminum influences cell culture, which has been found to have a superhydrophilic surface in anodized aluminum [19]. In addition, the thermal performance test shows that the micro/nano-textured morphology of the anodized aluminum surface increases the heat transfer performance with the increase of the nanotube in the alumina layer (diameter and length of the pores) [20].

Anodic sulfuric oxidation (ASO) electrolytically forms a layer of alumina on the surface, effectively protecting alloys from corrosion [21], and this process results from the combination of aluminum and oxygen released [22].

Chromatic anodic oxidation (CAO) results in the formation of a thin film in the micrometer thickness and good rubbability [23]; therefore, it provides excellent corrosion protection. Due to the recommendation of environment and health (Reach 2016), several researches were carried out to replace and substitute it with molybdates, tungstates, permanganates, and vanadates, including chemical elements similar to chromium (groups VB, VIB, and VIIB of the periodic table) [24].

Molybdate anodic oxidation (MoAO) is widely used as a treatment meeting the environmental requirement for aluminum alloys with low toxicity under various conditions. Molybdate ions also show good inhibition in acidic solution and NaCl solution [25, 26]. The layer formed is characterized by the presence of numerous fine pores [27]. These pores are the subject of a lot of works such as the research done by De Bonfils-Lahovary and Tao [28, 29], from which it was concluded that the pores are not a form of surface cracking [30], but this surface porosity results from the loss of aluminum cations to the electrolyte [17].

An artificial layer of phosphate (PCC) and molybdate (MCC) conversion coating is commonly used to replace chromate conversion coating (CCC) [31]. The layer formed during MCC is considered as an insulating layer thanks to the oxidability of molybdate ions ( $\text{MoO}_4^{2-}$ ) and the reducibility of the Al substrate [32].

In this work, we study the effect of the combination of the two treatment processes. First, for the anodization as well as the conversion coating to have a durable and effective protection moreover to meet the requirement of REACH (Registration, Evaluation and

Authorization of Chemicals), we choose a molybdate-based treatment. This study is therefore composed of two parts: the first is to study the treatments of anodization of A2030 alloy in the bath of molybdate (MoAO) without and with phosphoric acid in different concentrations and, secondly, the implementation of a treatment process including anodization, pre-oxidation, and conversion coating with molybdate. Optimal experimental conditions were determined to obtain films with good anti-corrosion performance.

## Material and methods

### Materials and pretreatment

The AA 2030 aluminum alloy with an exposed area of  $0.5\text{cm}^2$  sealed by epoxy resin was used in this work. The chemical composition of the samples (wt %) is Cu, 7.27; Mg, 1.46; Mn, 0.66; Si, 0.06; Fe, 0.21; Zn, 0.09; Ti, 0.04; Cr, 0.017; and Al, 90%. Before the electrochemical study, the surface of Al was polished with 600, 800, 1000, and 1200 grit sic abrasive paper, rinsed with bidistilled water, then degreased with acetone ethanol, deionized water, and dried with air flow, in order to remove the impurities residual from surfaces.

### Treatment solution

The treatment solution is prepared with three steps

\*First step (anodization):

- S1 is an anodization with different concentrations of sodium molybdate and bidistilled water.
- S2 is the combination of  $\text{Na}_2\text{MoO}_4$  with the different concentrations of phosphoric acid and bidistilled water.

The treatment lasts 45 min at room temperature, under a potential of  $14\text{ Volt/cm}^2$  and stirring at a low speed.

\*Second step (pre-oxidation):

- -S3: before the anodization of the alloy in S2, the pre-oxidation with 4% NaOH and bidistilled water at  $40^\circ\text{C}$  was carried out with different immersion times (30s, 60s, and 90s).

\*Finally (conversion coating):

- -S4: once the second step is completed (S3), a conversion with 0.4% sodium fluoride and 3% sodium molybdate at  $65^\circ\text{C}$  for 10min with pH 3 is initiated.

Electrochemical characterization is done in a solution that contains (wt %) 3.5% NaCl. Every experience is repeated twice and the average value is reported to reach reproducibility of results.

### Characterizations of the oxide layer and corrosion products

For the characterization of oxide layers formed after treatment, scanning electron microscopy (SEM), energy dispersive X-ray (EDS) spectrum analysis, AFM, and nano-indentation are required.

### Electrochemical measurements

For the characterization of the oxide layer formed on the Al surface with an area of about  $0.5 \text{ cm}^2$ , we used electrochemical studies, in an aggressive solution of 3.5% NaCl (% by weight) as an analyzer. The tests are carried out in a cell with three electrodes: aluminum as the working electrode (WE), Ag/AgCl as the reference electrode (RE), and platinum as the counter electrode (CE); the electrochemical workstation is Princeton Applied Research (VersaSTAT 3F, AMETEK). Before starting the electrochemical tests, the working electrodes (WE) should be immersed in the aggressive solution for a few minutes to have a more stable potential during the open circuit potential test (OCP). Electrochemical impedance spectroscopy (EIS) was performed over a frequency range from 100 kHz to 10 mHz with an excitation signal of 10 mV (RMS). The potentiostatic polarization (Tafel) measurements were measured from the cathodic to the anodic branch at  $\pm 250 \text{ mV}$  around OCP with a scan rate of 1 mV/s. Electrochemical parameters such as current density, anode, and cathode slope (ba and bc) were determined using Tafel plots.

## Results and discussion

### Surface analysis

#### Surface morphology

Scanning electron microscopy (SEM) images of the surface after treatment with S3 and S4 are shown in Fig. 1. In Fig. 1a, the surface of the alloy treated in S3 appears homogeneous with the presence of fine pores and the lines observed are due to mechanical polishing. This anodizing treatment is schematized in Fig. 2 and well explained by the following reactions:

- Cathode:



- Anode:



Then:

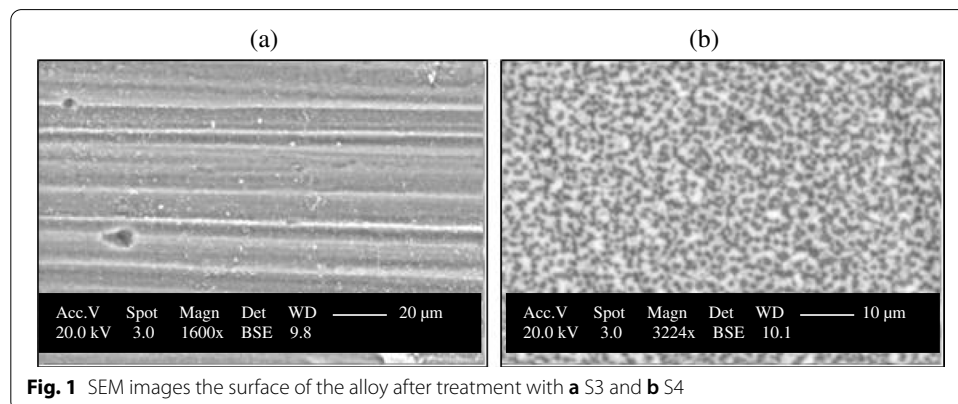
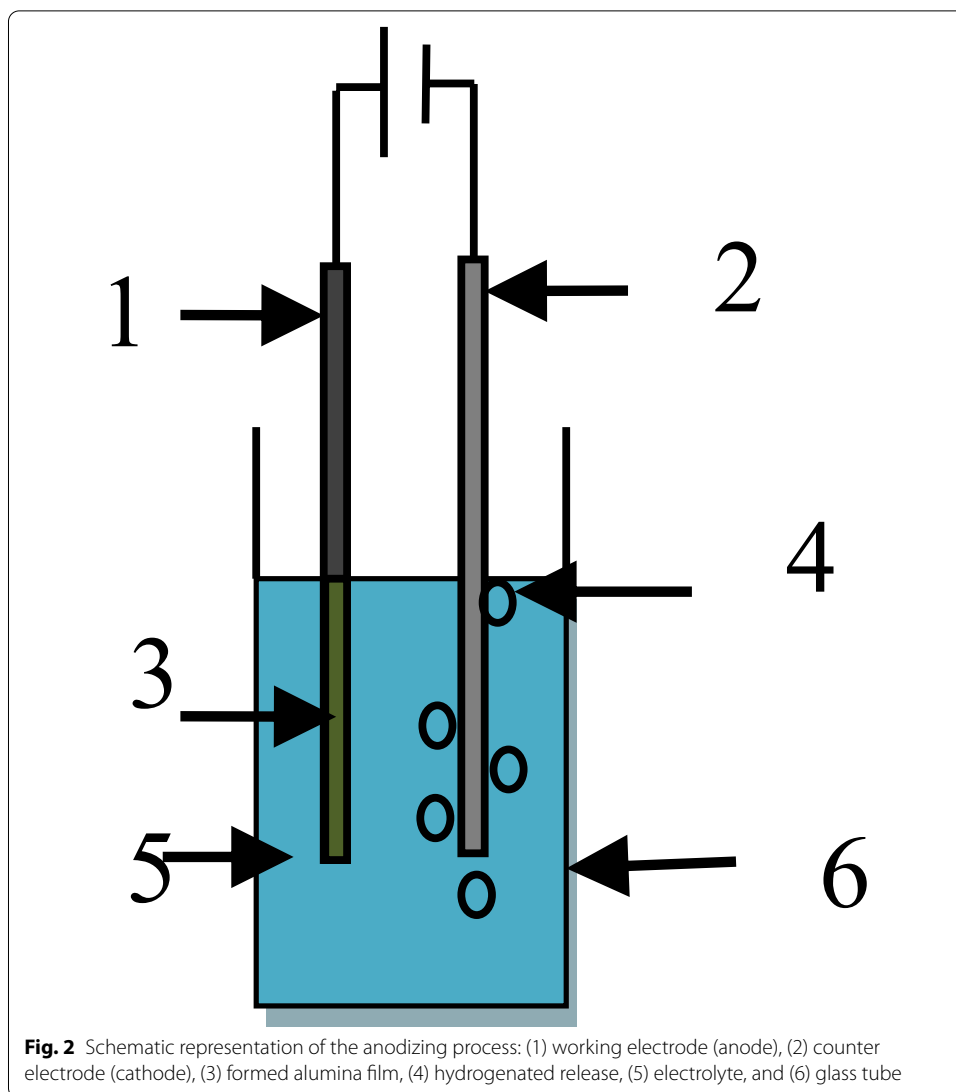
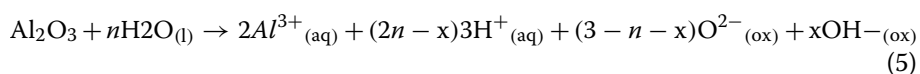
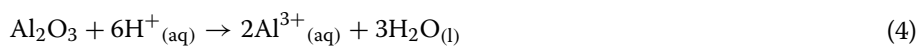


**Fig. 1** SEM images the surface of the alloy after treatment with **a** S3 and **b** S4



The layer of aluminum oxide formed above the metal corresponds to reactions 2 and 3, where the reduction of hydrogen at the cathode is presented in reaction 1, and the oxidation of aluminum at the level of anode by reaction 2, which causes the formation of the protective layer of alumina [33, 34].

The surface morphology of the alloy after S4 treatment with a conversion in pH=4 is shown in Fig. 3; the latter shows that the increase in pH causes the formation of a cracked and less adherent oxide layer. Figure 4 explains this mechanism of corrosion by a series of reactions:



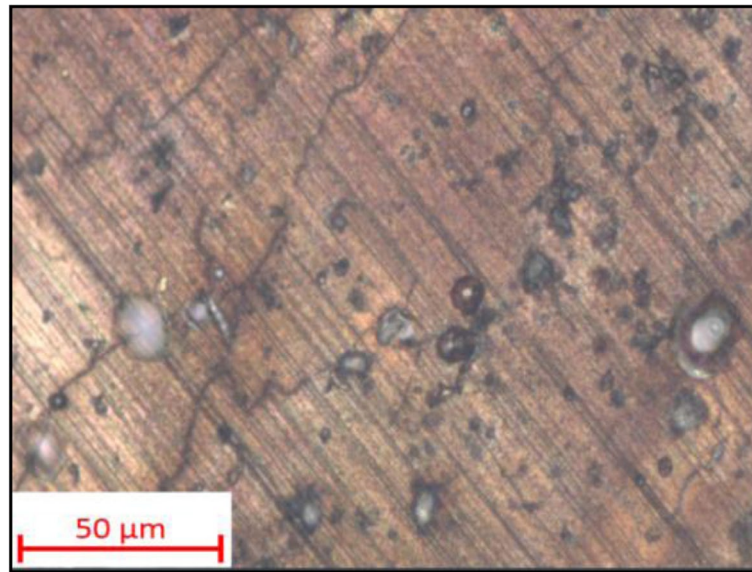


**Fig. 3** Surface morphology of the alloy after S4 treatment with conversion in pH4

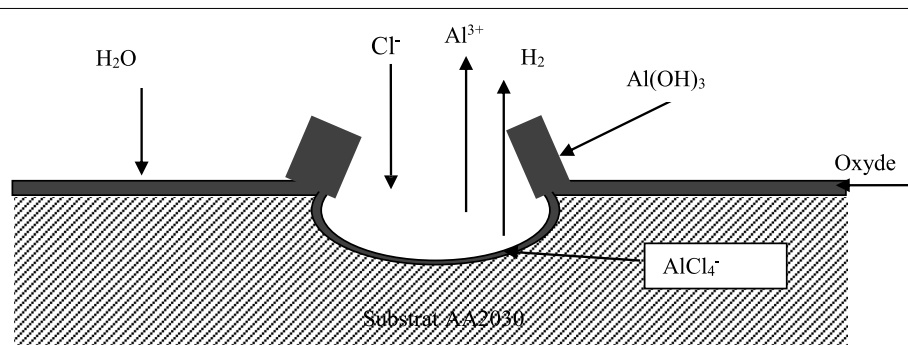


**Fig. 4** Schematic representation of the corrosion process

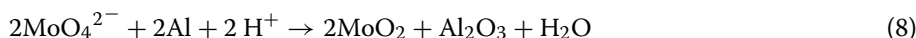
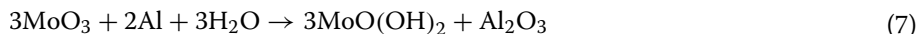
Reactions 4 and 5 explain the dissolution of the alumina layer, where  $n$  shows the amount of water separated per mole of  $\text{Al}_2\text{O}_3$  [30]. Localized corrosion is the most common phenomenon for aluminum alloys, which is due to their heterogeneous microstructure [35, 36].

After the treatment with S4 shown in Fig. 4b, a uniform non-porous layer is observed on the alloy, and its morphology is flake-like. According to Wang et al., the coating reacts with the high bath temperature to form boehmite products which penetrate into the pores and produce a flake-like cluster  $\text{AlOOH}$  as reaction 6 [37].



Figure 5 shows the nanopores formed in the oxide layer after anodization and conversion coating; these pores contain an inner layer containing pure alumina and an outer layer containing alumina contaminated with anions [38]. The absorption of molybdate at the aluminum surface causes the formation of conversion coatings

above the metal [33]; this mechanism is explained in reactions (7) and (8) and then in Fig. 5.



According to Bai et al. [38], we can explain the formation mechanism coating with two processes: treatment by the molybdate ions are absorbed on the surface then the absorbed ions react with the aluminum substrate to form conversion coatings.

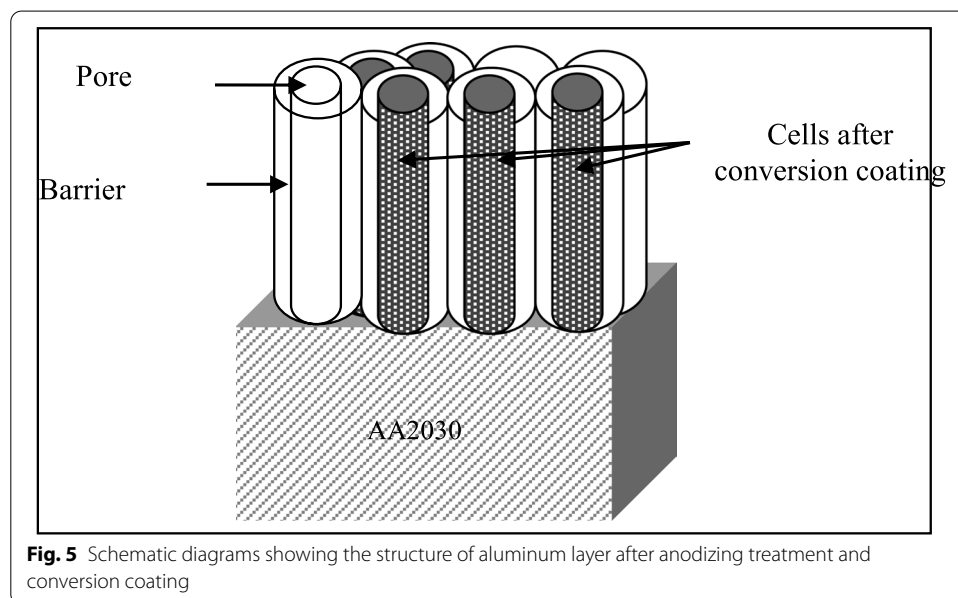
Two different reactions are considered occurring on the surface: one is that molybdate ions react with  $\text{H}^+$  existing on the interface of metal and solution to form molybdic acid and the latter hydrolyzes to form  $\text{MoO}_3$ . The  $\text{MoO}_3$  will react with the aluminum to form  $\text{MoO}(\text{OH})_2$ . The reaction continues until the resultant  $\text{MoO}_3$ ,  $\text{MoO}_2$ , and  $\text{MoO}(\text{OH})_2$  cover the whole surface. So the constituents of the conversion coatings are mainly  $\text{MoO}_3$ ,  $\text{MoO}_2$ , and  $\text{MoO}(\text{OH})_2$ .

The addition of  $\text{F}^-$  facilitates the surface reaction of aluminum alloy through the following reaction: (9). Due to the relatively weak oxidizability of molybdate ions, the chemical conversion coatings deposited directly on the aluminum alloy surface usually have weak adhesion force with the substrate but the use of a porous surface. Figure 5 helps to form more adhesive coatings [39].



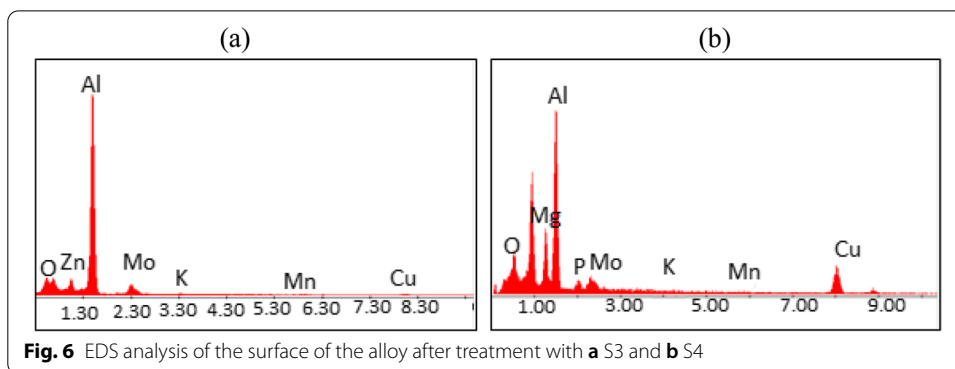
### EDS spectra

Figure 6 shows the energy dispersive X-ray spectra (EDS) of the different treatments S3 and S4 respectively. The chemical composition of the oxide layer after S3 and S4 treatment is summarized in Tables 1 and 2 respectively.



**Fig. 5** Schematic diagrams showing the structure of aluminum layer after anodizing treatment and conversion coating





**Fig. 6** EDS analysis of the surface of the alloy after treatment with **a** S3 and **b** S4

**Table 1** The chemical composition of the oxide layer after two-step treatment

Elements	O	Zn	Mg	Al	P	Mo	K	Mn	Cu
Weight %	20.27	0.50	1.85	68.91	1.38	3.52	0.23	0.64	2.69
Atomic %	31.32	0.19	1.88	63.12	1.10	0.91	0.14	0.29	1.05

**Table 2** The chemical composition of the oxide layer after three-step treatment

Elements	O	Mg	Al	P	Mo	K	Mn	Cu
Weight %	18.29	13.28	34.12	2.00	6.47	0.26	0.50	25.08
Atomic %	32.69	15.63	36.17	1.85	1.93	0.19	0.26	11.29

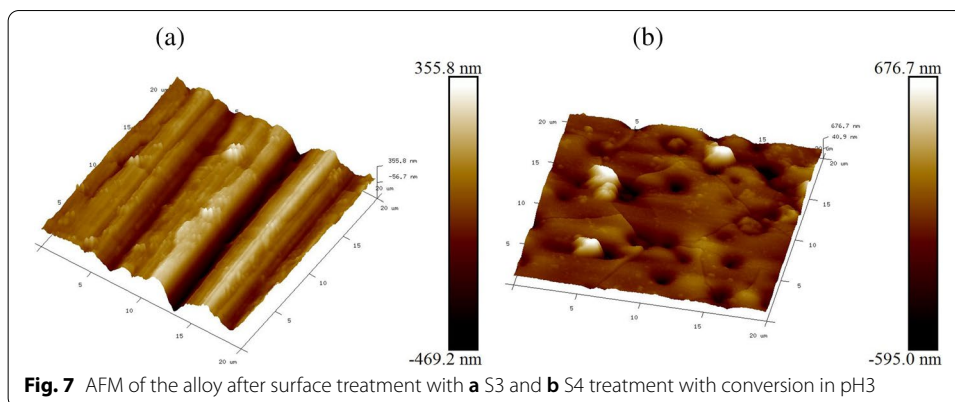
According to these results, the existence of molybdate (3.5%) was observed on the surface of the AA2030 alloy treated in S3, due to the composition of the anodizing bath. On the other hand, the appearance of an increase of molybdate (6.47%) after the S4 treatment confirms the formation of a molybdate conversion coating (MCC), and this indicates that the S4 treatment is beneficial for the formation of MoO<sub>2</sub> and Al<sub>2</sub>O<sub>3</sub>. The increase in copper illustrates the increase in the corrosion resistance of the layer formed during the treatment in S4.

**Atomic force microscopy**

Atomic force microscopy (AFM) is an effective and in situ method to acquire the surface morphology with high resolution. Figure 7 is the micrograph of the studied area of the signal line with dimensions of 20 × 20 μm<sup>2</sup>. It presents the 3D graph of the alloy after surface treatment in (a) S3 and (b) S4.

It can be deduced from Fig. 7a and b the layer morphology formed after treatment in S3 and S4 for 2030 aluminum alloy, which has a homogeneous distribution. Figure 7a shows needle-like small grain structures formed on the alloy treated in S3 with some scratches due to polishing and with an average surface roughness of 82.9 nm. The image





in Fig. 7b appears relatively and evenly flat and smooth with an average surface roughness of 89.3 nm. The surface roughness of the alloy substrate is increased after the last processing step (S4) by the physical interactions, which improves the adhesion property of the coating to the material surface [40]; in addition, the electrical resistance decreases when the contact area increases [41, 42]. Consequently, the Al treated in S4 could be considered as an efficient treatment to prevent corrosion.

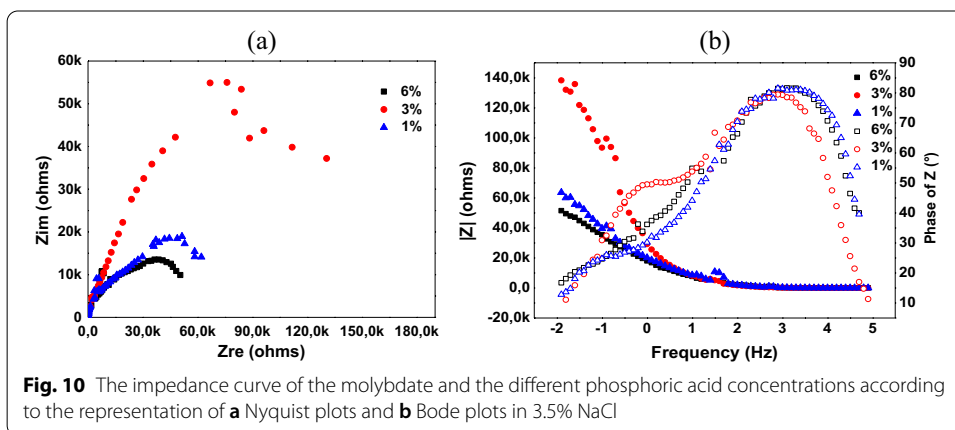
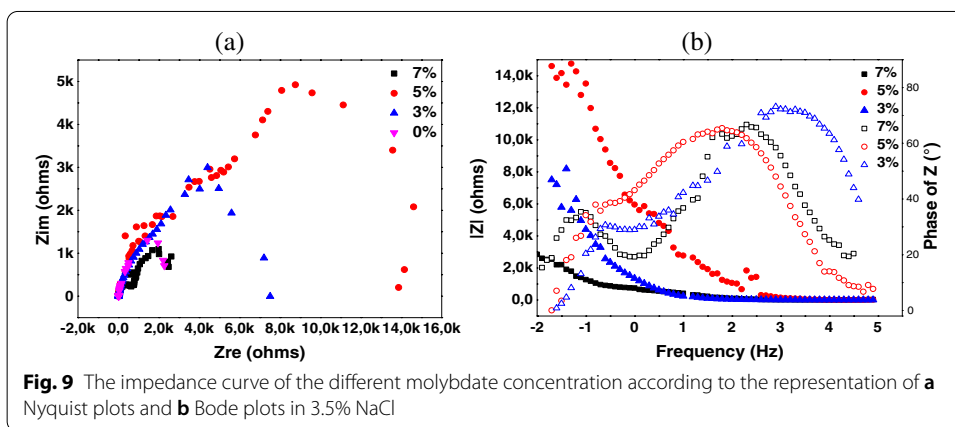
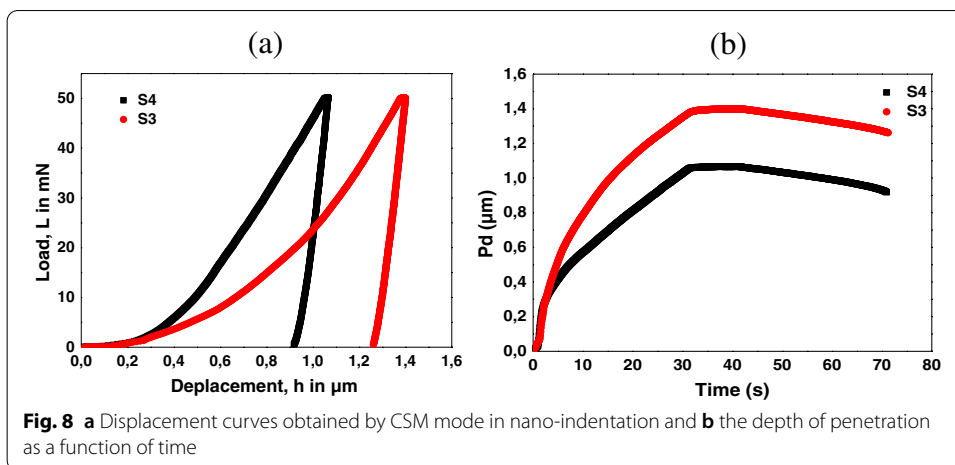
#### **Nano-indentation**

Nano-indentation is a very important analysis technique to determine the elasticity modulus of the film formed on the aluminum alloy [43]. The contact with the penetrator and the material surface during nano-indentation results in the recording of the load depth and indentation with high electronic precision which leads to the deformation of elastics in the material [44]. This technique allows the characterization of oxide layers by determining the modulus of elasticity of the film [45, 46]. Its value can also be determined using an Oliver and Pharr technique which is one of the most important techniques [47].

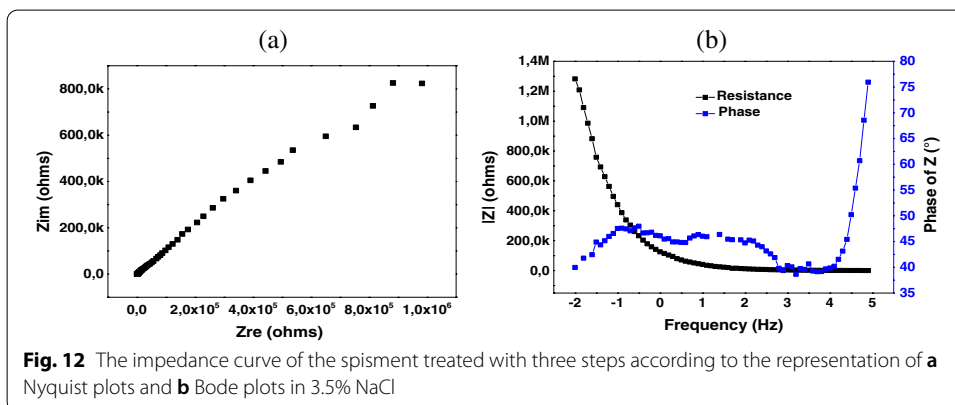
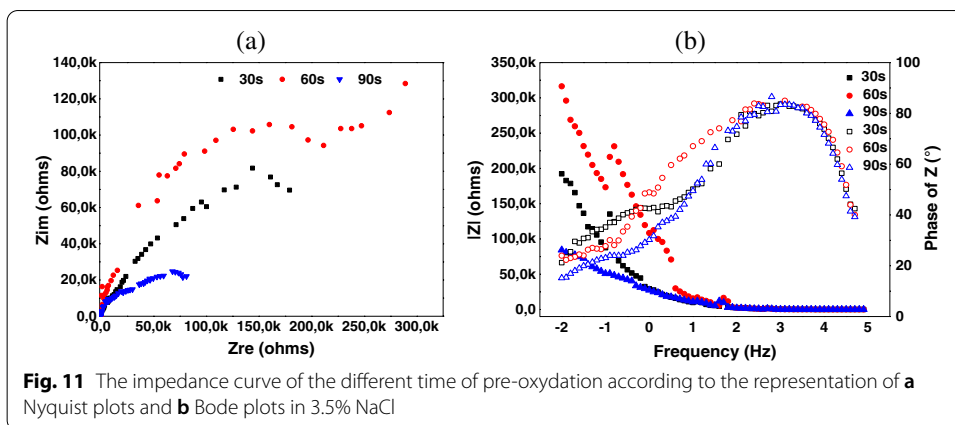
Figure 8 shows low displacement curves obtained by CSM mode in nano-indentation (a) and the depth of penetration as a function of time (b). After the same time and with the application of a constant load between 10 and 50 mN, the same phenomenon is observed for the two curves representing the S3 and S4 treatment, that is the increase of the penetration depth in parallel with the increase of the load and the time; on the other hand, in the curve of the sample treated in S3, the penetrator penetrates deeper compared to the one treated in S4; moreover, the displacement of the maximum fast load for the alloy treated in S4 is 900nm compared to that treated in S3 which is 1250nm, and the modulus of elasticity improves from 59 to 82 GPa during the treatment in S3 and S4 respectively. From this, it is concluded that the layer formed in S4 is more hard.

#### **Electrochemical impedance spectroscopy (EIS)**

The impedance spectra recorded for the AA2030 alloy according to the Nyquist representation after different treatments are shown in Figs. 9, 10, 11, and 12 (a). Figure 9a shows the different percentages of molybdate concentration, and the spectrum is characterized by a well-defined capacitive loop in the high-frequency range, which represents the interface reaction between the electrolyte solution and the substrate. Figure 10a



shows the impedance diagrams of the samples treated with 5% Mo and with a variation of the percentage of phosphoric acid. These show two capacitive loops in the high-frequency ranges for 6% and 1% phosphoric acid. The curve for 3% phosphoric acid shows a capacitive loop with the highest resistance part in the impedance diagram. Figure 11a is



characterized by the value of the resistive part for the 60-s pre-oxidation time which has the largest capacitive loop. It is important to note that the inductive response was not observed for the treated samples. It is well known that the larger diameter of the semi-circle, the corrosion resistance of the sample is better. In this way, the responses of the treated samples show larger semi-circles compared to the S1 samples, confirming that all treatments improve the corrosion resistance of the AA2030 alloy in 3.5% NaCl solution.

According to previous studies [48], the capacitive loops for the samples in the high-frequency range correspond to the charge transfer resistance on the substrate surface (R) and the capacitance (C). The low-frequency capacitive loop is attributed to the corrosion product layer, oxide film, and coating on the surface of the metal substrate but the absence of this phenomenon in Fig. 12a proves that the treatment has a compact layer. In summary, it is clear from Fig. 13 that the S4 treatment offers superior anti-corrosion performance for the AA2030 alloy.

Phosphate and molybdate ions can form heteropoly acid phosphorus-molybdate in the acid solution, which has strong oxidizing properties. Therefore, we assume that they will be bound together in a certain proportion, and phosphorus-molybdate can modulate the rate of oxide film formation and lead to improved resistance [49].

The Bode diagram shown in Figs. 9, 10, 11, and 12 (b) presents the variation of the impedance amplitude and phase angle. According to the literature, the impedance

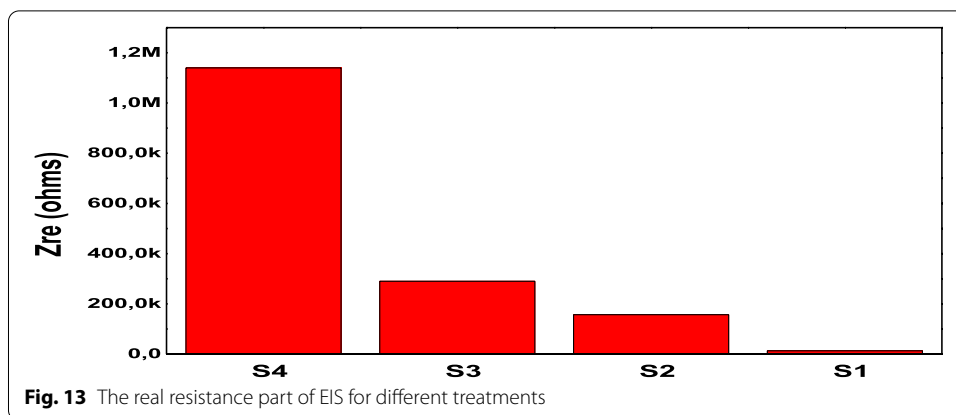


**Table 3** Impedance parameters derived from EIS fitting curves for aluminum alloy 2030 in 3.5% NaCl for the different treatment baths

Treatment	S0	S1	S2	S3	S4
R <sub>0</sub> (ohm)	2271.14	/	/	/	/
R <sub>p</sub> (ohm)	/	13213	1.57e+05	2.9e+05	1.14e+06
R <sub>s</sub> (ohm)	/	22.119	17.498	22.122	75.095
η	/	82.81	98.55	99.21	99.80

spectrum at high frequency reflects the characteristics of the porous layer of the film, while at low frequency reflects the characteristics of the barrier layer. Seen in the Bode diagram, the impedance modulus increases from S1 to S4, and the phase angles are positive so that their growth is parallel with the growth of the frequency which means that the treatment is improved with a compact layer.

The inhibition efficiency (η) was calculated from the Nyquist diagram by the polarization resistance R<sub>p</sub>, as in the following equation:

$$\eta = \frac{(R_p - R_0)}{R_p} \times 100$$

The impedance parameters were derived from the EIS fitting curves for aluminum alloy 2030 in 3.5% NaCl for the different treatment baths and are listed in Table 3 where R<sub>set</sub> and R<sub>0</sub> were the solution resistance and the blank resistance respectively.

In accordance with Table 3, the inhibition efficiency was increased in parallel with the polarization resistance (R<sub>p</sub>) to more than 99.8% at S4, confirming the excellent effect of the bath (S4) which combines between two corrosion treatment processes < anodizing and conversion coating > with the same inhibitor < sodium molybdate > for aluminum alloy 2030 in 3.5% NaCl.

**Potentiodynamic polarization curve (Tafel)**

The polarization curves of the aluminum alloy for the different treatment steps are shown in Fig. 14. Hence, the values of the corrosion potential (E<sub>corr</sub>) and the corrosion current density (I<sub>corr</sub>) are key parameters for assessing the corrosion behavior of the films formed after the different treatments.

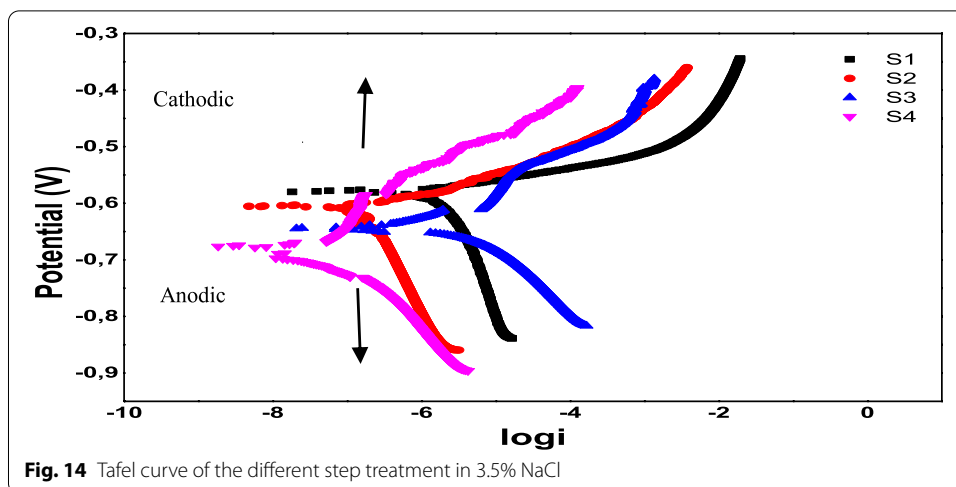


**Table 4** Corrosion parameters of anodic oxidation films formed in the presence of various steps

	One step		Two steps	Three steps
	S1	S2	S3	S4
Ba	17.12	22.75 8	56.317	111.89
Bc	30.958	26.84	24.11	58.82
$I_0$ (A/cm <sup>2</sup> )	3.81E-07	1.76E-07	4.62E-7	3E-08
$E_0$	-0.57	-0.60	-0.64	-0.69

Table 4 reports the values related to the estimation of the corrosion parameters ( $E_{corr}$ , cathodic (Bc), and anodic (Ba) tafel slopes and the corrosion current density ( $i_{corr}$ )) for all the treatments studied. In Fig. 14, we observe dissolution of the anode for the aluminum alloy sample treated in baths S1 and S2, while for the sample treated in the other baths, the corrosion potential decreases and moves towards an anodic potential which causes the passivation of the anode. The anode slopes for the different treatments increase while the current density decreases which improves the anti-corrosion property of the aluminum alloy [50]. The polarization curve shows that oxygen diffusion controls the cathodic process of the S1 and S2 aluminum alloy in aggressive solution, while that of the S4-treated sample is controlled by an electrochemical process, during which the action of oxygen is effectively inhibited and thus the cathodic reaction and the corrosion rate have decreased, and these results confirm what has been obtained in electrochemical impedance spectroscopy studies, by estimating the positive effect of the S4 bath. To characterize the anti-corrosion properties of the oxide layer, the corrosion potential ( $E_{corr}$ ) increased from  $-0.57V$  for S3 to  $-0.69V$  for S4 and a significant improvement in corrosion performance is observed for the S4 treatment, which has the lowest  $I_{corr}$  of  $3E-08$  among all samples. In general, it has been reported that low  $I_{corr}$  leads to a low corrosion rate and good polarization resistance ( $R_p$ ) of the coatings [51, 52].

## Conclusions

In this work, we studied the effect of anodization, pre-oxidation, and conversion of 2030 T3 aluminum alloys on corrosion with environmental-friendly molybdate.

Electrochemical methods including EIS and Tafel have been adopted to comprehensively assess the corrosion behavior of AA2030. In addition, AFM, SEM/EDS, and nano-indentation were used to detect the composition and morphology of oxide layers formed on the surface of the alloy. The electrochemical data correlated with alloy microstructure and layer composition, and for that, we conclude:

1. Sodium molybdate treatment at 5% concentration effectively inhibits corrosion of AA2030, as it acts as an anodic inhibitor. The latter offers good protection in the treatment with the addition of 3% phosphoric acid and their synergistic effect reduces defects in the anode oxidation film. The addition of the pre-oxidation to the treatment improved considerably the efficiency of inhibition.

2. Thus, although the previous treatment improved the corrosion resistance of anodizing aluminum, fine pores were still observed at the nanoscale, and the addition of molybdate conversion coating (MCC) favored the generation of a compact and protective layer, which effectively prevent aggressive attacks on the substrate and speedily consumption of the oxide layer; moreover, S4 provided excellent corrosion resistance in the  $10^6$ -ohm range with an efficiency of 99.8%.

3. The results of the nano-indentation show that the layer formed on the alloy treated in S4 is hard, due to the presence of molybdate which has characteristics of inhibitions against corrosion and mechanical properties against wear.

Accordingly, the elaborated procedure presents a means of improving the strength and inhibiting the corrosion of aluminum alloys in a saline environment.

## Abbreviations

REACH: Registration Evaluation and Authorization of Chemicals; ASO: Anodic sulfuric oxidation; CAO: Chromatic anodic oxidation; MoAO: Molybdate anodic oxidation; MCC: Molybdate conversion coating; PCC: Phosphate conversion coating; CCC: Chromate conversion coating.

## Acknowledgements

Not applicable

## Disclosure statement

No potential conflict of interest was reported by the authors.

## Authors' contributions

The research reported in this paper was conceptualized by MB. The methodology was suggested by AH, AB, and SY. The manuscript was prepared by MB. AH, AB, and SY supervised the research. All the authors read and approved the final manuscript.

## Funding

We declare that we have no funding that may inappropriately influence our work presented in the manuscript titled "The effect of inhibiting molybdate used in anodizing-conversion treatment to improve corrosion protection of AA2030 aluminum alloy in different step."

## Availability of data and materials

The datasets used and analyzed during the current study are available from the corresponding author on reasonable request.

## Declarations

### Competing interests

The authors declare that they have no competing interests.

**Author details**

<sup>1</sup>University M'hamed Bougara, Faculté des Sciences de l'Ingénieur (Campus ouest–Boumerdès) Cité Frantz, Fanon 35000 Boumerdès, Algeria. <sup>2</sup>Research Center in Industrial Technologies CRTI, BP 64, Route de Dely Brahim, Algier 16014 Chérag, Algeria. <sup>3</sup>University of Science and Technology Houari Boumediene, 16000 Bab Ezzouar, Algier, Algeria.

Received: 16 January 2022 Accepted: 23 March 2022

Published online: 04 May 2022

**References**

1. Rashid KH, Khadom AA, Mahood HB (2020) Aluminum ASA 6061 anodizing process by chromic acid using Box–Wilson central composite design: optimization and corrosion tendency. *Met. Mater. Int.* <https://doi.org/10.1007/s12540-020-00762-1>
2. Laleh RR, Savaloni H, Abdi F, Abdi Y (2019) Corrosion inhibition enhancement of Al alloy by graphene oxide coating in NaCl solution. *Prog Org Coat.* 127:300–307 (<https://doi.org/10.1016/j.porgcoat.2018.11.03>)
3. Ashtiani HRR, Shahsavari P (2016) Strain-dependent constitutive equations to predict high temperature flow behavior of AA2024 aluminum alloy. *Mech Mater.* 100:209–218 <https://doi.org/10.1016/j.mechmat.2016.06.0178>
4. Chung IM, Malathy R, Kim SH, Kalaiselvi K, Prabakaran M, Gopiraman M (2020) Ecofriendly green inhibitor from *Hemerocallis fulva* against aluminum corrosion in sulphuric acid medium. *J Adhes Sci Technol.* 1–24. <https://doi.org/10.1080/01694243.2020.1712770>.
5. Wang J, Xiong F, Liu H, Zhang T, Li Y, Li C, Xia W, Wang H, Liu H (2019) Study of the corrosion behavior of *Aspergillus niger* on 7075-T6 aluminum alloy in a high salinity environment. *Bioelectrochemistry* 129:10–17 <https://doi.org/10.1016/j.bioelechem.2019.04.020>
6. Hongyang Wang, Xiaoxue Zhang, Xu Peng, Liqun Luo & Leiting Shen (2021) Comprehensive recovery of aluminum and calcium from aluminum-anodizing sludge by physicochemical process. *J Sustain Metallurgy* 7;1343. <https://doi.org/10.1007/s40831-021-00426-3>.
7. Li Y, Li J, Huang M, Xiang Y, Yang Y (2019) Effect of combined surface treatment on the adhesion performance of aluminium–lithium alloy. *J Adhesion Sci Technol.* 1–15. <https://doi.org/10.1080/01694243.2019.1613947>.
8. Jensen F, Kongstad I, Dirscherl K, Gudla VC, Ambat R (2019) High frequency pulse anodising of recycled 5006 aluminium alloy for optimised decorative appearance. *Surf Coat Technol.* 368:42–50 <https://doi.org/10.1016/j.surfcoat.2019.04.024>
9. Zhang P, Zu Y (2019) Effects of pore parameters on performance of anodic film on 2024 aluminum alloy. *Mater. Chem. Phys.* 231:9–20 <https://doi.org/10.1016/j.matchemphys.2019.04.008>
10. Salstela J, Suvanto M, Pakkanen TT (2016) Influence of hierarchical micro-micro patterning and chemical modifications on adhesion between aluminum and epoxy. *Int J AdhesAdhes* 66:128–137 <https://doi.org/10.1016/j.ijadhadh.2015.12.036>
11. Wang X, Lin J, Min J et al (2018) Effect of atmospheric pressure plasma treatment on strength of adhesive-bonded aluminum AA5052. *J Adhesion* 94:701–722 <https://doi.org/10.1080/00218464.2017.1393747>
12. Robaidi AA, Anagreh N, Massadeh S et al (2011) The effect of different surface pretreatment methods on nano-adhesive application in high strength steel and aluminum bonding. *J Adhes Sci Technol* 25:1725–1746 <https://doi.org/10.1163/016942410x535046>
13. Yang S, Li S, Meng Y, Yu M, Liu J, Li B (2021) Corrosion inhibition of aluminum current collector with molybdate conversion coating in commercial LiPF<sub>6</sub>-esters electrolytes. *Corrosion Science* 190:109632 <https://doi.org/10.1016/j.corsci.2021.109632>
14. Lin CW, Lai YC, Liu SS (2001) Effect of the surface roughness of sulfuric acid-anodized aluminum mold on the interfacial crystallization behavior of isotactic polypropylene. *J Adhes Sci Technol* 15(8):929–944 <https://doi.org/10.1163/15685610152542379>
15. Ma Y, Wen Y, Li J, Feng C, Zhang Z, Gou T, Huang J, Lu J, Cui Z, Sun R (2020) Fabrication of alumina with ordered tapered-nanopore nested in micro-bowl hierarchical structure by a combined anodization. *Mater Chem Phys.* 239:122023 <https://doi.org/10.1016/j.matchemphys.2019.12>
16. Saeedikhani M, Javidi M, Vafakhah S (2017) Anodising of 2024-T3 aluminum alloy in electrolyte of sulphuric–boric–phosphoric mixed acid containing cerium salt as corrosion inhibitor. *Trans Nonferrous Met Soc China* 27711–721. [https://doi.org/10.1016/S1003-6326\(17\)60079-7](https://doi.org/10.1016/S1003-6326(17)60079-7)
17. Fadillah L, Takase K, Kobayashi H, Turczyniak-Surdacka S, Strawski M, Kowalski D, Zhu C, Aoki Y, Habazaki H. (2019) The role of tungsten species in the transition of anodic nanopores to nanotubes formed on iron alloyed with tungsten. *Electrochimica Acta* 309:274–282. <https://doi.org/10.1016/j.electacta.2019.03.206>.
18. Chien Y-C, Weng HC (2021) Cost-effective technique to fabricate a tubular through-hole anodic aluminum oxide membrane using one-step anodization. *Microelectron Eng.* 247:111589 <https://doi.org/10.1016/j.mee.2021.111589>
19. Yen M-L, Hsiao H-M, Huang C-F, Lin Y, Shen Y-K, Tsai Y-L, Chang C-W, Yen H-J, Lu Y-J, Kuo Y-W (2017) Aluminum templates of different sizes with micro-, nano- and micro/nano-structures for cell culture. *Coatings* 7(11):179 <https://doi.org/10.3390/coatings7110179>
20. Weng H, Yang M-H (2018) Heat transfer performance enhancement of gravity heat pipes by growing AAO nanotubes on inner wall surface. *Inventions* 3(3):42 <https://doi.org/10.3390/inventions3030042>
21. Moon S, Nam Y, Yang C, Jeong Y (2011) Growth of anodic oxide films on AC2A alloy in sulphuric acid solution. *Corros Sci.* 53:1547–1553 <https://doi.org/10.1016/j.corsci.2011.01.029>
22. Nettikaden VC, Liu H, Skeldon P, Thompson GE (2012) Porous anodic film formation on Al–Ti alloys in sulphuric acid. *Corros Sci.* 57:49–55 <https://doi.org/10.1016/j.corsci.2011.12.035>



23. Elabar D, Němcová A, Hashimoto T, Skeldon P, Thompson GE (2015) Effect of sulphate impurity in chromic acid anodizing of aluminium. *Corros Sci.* 100:377–385 <https://doi.org/10.1016/j.corsci.2015.08.019>
24. Wan TT, Liu ZX, Bu MZ, Wang PC (2013) Effect of surface pretreatment on corrosion resistance and bond strength of magnesium AZ31 alloy. *Corros Sci.* 66:33–42 <https://doi.org/10.1016/j.corsci.2012.08.051>
25. Wang, D.; Wu, M.; Ming, J.; Shi, J (2020) Inhibitive effect of sodium molybdate on corrosion behaviour of AA6061 aluminium alloy in simulated concrete pore solutions. *Constr Build Mater.* 121463. <https://doi.org/10.1016/j.conbuildmat.2020.121463>.
26. Kharitonov DS, Dobryden I, Sefer B, Ryl J, Wrzesińska A, Makarova IV, Bobowska I, Kurilo II, Claesson PM (2020) Surface and corrosion properties of AA6063-T5 aluminum alloy in molybdate-containing sodium chloride solutions. *Corros Sci.* 171:108658 <https://doi.org/10.1016/j.corsci.2020.108658>
27. Lee W, Park SJ (2014) Porous anodic aluminum oxide: anodization and templated synthesis of functional nanostructures. *Chemical reviews* 114:7487–7556 <https://doi.org/10.1021/cr500002>
28. De Bonfils-Lahovary ML, Josse C, Laffont L, Blanc C (2019) Influence of hydrogen on the propagation of intergranular corrosion defects in 2024 aluminum alloy. *Corros Sci.* 148, 198–205. <https://doi.org/10.1016/j.corsci.2018.12.019>.
29. Tao Y, Xiong T, Sun C, Kong L, Cui X, Li T, Song GL (2010) Microstructure and corrosion performance of a cold sprayed aluminum coating on AZ91D magnesium alloy. *Corros Sci.* 52:3191–3197 <https://doi.org/10.1016/j.corsci.2010.05.023>
30. Zhang S, Zhang T, He Y, Feng Y, Du X, Ma B, Zhang T (2019) Effect of coastal atmospheric corrosion on fatigue properties of 2024-T4 aluminum alloy structures. *J Alloys Compd.* 802:511–521 <https://doi.org/10.1016/j.jallcom.2019.06.235>
31. Yang S, Li S, Meng Y, Yu M, Liu J, Li B (2021) Corrosion inhibition of aluminum current collector with molybdate conversion coating in commercial LiPF<sub>6</sub>-esters electrolytes. *Corros Sci.* 190:109632 <https://doi.org/10.1016/j.corsci.2021.109632>
32. Kwolek P, Kaminski A, Dychton K, Drajewicz M, Sieniawski J (2016) The corrosion rate of aluminium in the orthophosphoric acid solutions in the presence of sodium molybdate. *Corros Sci.* 106:208–216 <https://doi.org/10.1016/j.corsci.2016.02.005>
33. Sousa CT, Leitao DC, Proenca MP, Ventura J, Pereira AM, Araujo JP (2014) Nanoporous alumina as templates for multifunctional applications. *Appl Phys Rev.* 1:3 <https://doi.org/10.1063/1.4893546>
34. Benmohamed M, Benmounah A, Haddad A (2020) Effect of different anodizing bath on improving the corrosion resistance of a 2030 aluminum alloy. *Proceedings of the 4<sup>th</sup> International Symposium on Materials and Sustainable Development* 13–25.
35. Datta J, Samanta B, Jana A, Sinha S, Bhattacharya C, Bandyopadhyay S (2008) Role of Cl<sup>-</sup> and NO<sub>3</sub><sup>-</sup> ions on the corrosion behavior of 20% SiC reinforced 6061-Al metal matrix composite: a correlation between electrochemical studies and atomic force microscopy. *Corros Sci.* 50:2658–2668 <https://doi.org/10.1016/j.corsci.2008.06.027>
36. Zhang Z, Liu F, Han EH, Xu L, Uzoma PC (2019) Effects of Al<sub>2</sub>O<sub>3</sub> on the microstructures and corrosion behavior of low-pressure cold gas sprayed Al 2024-Al<sub>2</sub>O<sub>3</sub> composite coatings on AA 2024-T3 substrate. *Surf Coat Technol.* 370:53–68 <https://doi.org/10.1016/j.surfcoat.2019.04.082>
37. Wang R, Wang L, He C, Lu M, Sun L (2018) Studies on the sealing processes of corrosion resistant coatings formed on 2024 aluminium alloy with tartaric-sulfuric anodizing. *Surf Coat Technol.* 12.092. <https://doi.org/10.1016/j.surfcoat.2018.12.092>.
38. Bai, F.; Li, J.F.; Viehland, D (2004) Domain hierarchy in annealed (001)-oriented Pb( Mg 1 / 3 Nb 2 / 3 ) O 3 – x % PbTiO 3 single crystals. *Appl Phys Lett.* 85, 12. <https://doi.org/10.1063/1.1793353>.
39. Du SG, Yan J, Cui HP, Wang B (2008) Preparation of molybdate conversion coatings on the anodizing surface of aluminum alloy. *Key Eng Mater.* 368-372:1287–1290 <https://doi.org/10.4028/www.scientific.net/KEM.368-372.1287>
40. Zhu W, Li W, Mu S, Fu N, Liao Z (2017) Comparative study on Ti/Zr/V and chromate conversion treated aluminum alloys: anti-corrosion performance and epoxy coating adhesion properties. *Appl Surf Sci.* 405:157–168. <https://doi.org/10.1016/j.apsusc.2017.02.046>
41. Mao S, Li, W, Zeng X, Yi A, Liao Z, Zhu W (2020) Multiple transitional metal oxides conversion coating on AA6063 toward corrosion protection and electrical conductivity. *Surf Coat Technol.* 125819. <https://doi.org/10.1016/j.surfcoat.2020.125819>.
42. Wu X, Zhan L, Zhao X, Wang X, Chang T (2019) Effects of surface pre-treatment and adhesive quantity on interface characteristics of fiber metal laminates. *Composite Interfaces.* 1–15. <https://doi.org/10.1080/09276440.2019.1707023>.
43. Hemmouche L, Chicot D, Amrouche A, Iost A, Belouchrani MA, Decoopman X, Puchi-Cabrera ES (2013) An analysis of the elastic properties of a porous aluminium oxide film by means of indentation techniques. *Mater Sci Eng A.* 585:155–164 <https://doi.org/10.1016/j.msea.2013.07.054>
44. Khodabakhshi F, Gerlich AP, Verma D, Haghshenas M (2018) Nano-indentation behavior of layered ultra-fine grained AA8006 aluminum alloy and AA8006-B4C nanostructured nanocomposite produced by accumulative fold forging process. *Mater Sci Eng A.* 12:013 <https://doi.org/10.1016/j.msea.2018.12.013>
45. Tricoteaux A, Duarte G, Chicot D, Le Bourhis E, Bemporad E, Lesage J (2010) Depth-sensing indentation modeling for determination of elastic modulus of thin films. *Mech Mater.* 42(2), 166–174. <https://doi.org/10.1016/j.mechmat.2009.11.016>.
46. Batista JCA, Godoy C, Pintaúde G, Sinatora A, Matthews A (2003) An approach to elucidate the different response of PVD coatings in different tribological tests. *Surf Coat Technol.* 174-175, 891–898. [https://doi.org/10.1016/S0257-8972\(03\)00351-7](https://doi.org/10.1016/S0257-8972(03)00351-7).
47. Oliver WC, Pharr GM (1992) An improved technique for determining hardness and elastic modulus using load and displacement sensing indentation experiments. *J Mater Res* 7(06), 1564–1583. <https://doi.org/10.1557/JMR.1992.1564>.
48. Quebbou Z, Chafi M, Omari LE (2020) Corrosion resistance of 5005 aluminum alloy by anodizing treatment in a mixture of phosphoric and boric acids. *Mater Today Proc.* 08.406. <https://doi.org/10.1016/j.matpr.2020.08.406>.

49. Wang W, Dong P, Wang H, Cheng J, Liu S (2019) Synergistic corrosion inhibition effect of molybdate and phosphate ions for anodic oxidation film formed on 2024 aluminum alloy. *J Wuhan Univ Technol-Mater.* 34(2):426–432. <https://doi.org/10.1007/s11595-019-2069-z>.
50. Le Coz F, Arurault L, Datas L (2010) Chemical analysis of a single basic cell of porous anodic aluminium oxide templates. *Mater Charact.* 61:283–288. <https://doi.org/10.1016/j.matchar.2009.12.008>
51. Zhang Y, Yan C, Wang F, Lou H, Cao C (2002) Study on the environmentally friendly anodizing of AZ91D magnesium alloy. *Surf Coat Technol.* 161(1), 36–43. [https://doi.org/10.1016/S0257-8972\(02\)00342-0](https://doi.org/10.1016/S0257-8972(02)00342-0).
52. Sun X, Cao X, Zhang Z, Han X, Ruan H, Dong Z (2021) Synergistic inhibition of cerium and alkyl phosphate composite adlayer on pitting corrosion of Al–Mg–Si aluminium alloy. *Corrosion Eng Sci Technol.* 1–12. <https://doi.org/10.1080/1478422X.2021.1941542>.

### Publisher's Note

Springer Nature remains neutral with regard to jurisdictional claims in published maps and institutional affiliations.

**Submit your manuscript to a SpringerOpen<sup>®</sup> journal and benefit from:**

- ▶ Convenient online submission
- ▶ Rigorous peer review
- ▶ Open access: articles freely available online
- ▶ High visibility within the field
- ▶ Retaining the copyright to your article

---

Submit your next manuscript at ▶ [springeropen.com](https://www.springeropen.com)

---